



Report Number 09/20

**Pebble bed: reflector treatment and pressure  
velocity coupling**

by

**J.P.F. Charpin, N. S. Kobo, K. Legodi, O.D.  
Makinde, J.-M. T. Ngnotchouye, H. Ockendon,  
A. Z. Owinoh, S. Peppin, J. Whiteley**



Oxford Centre for Collaborative Applied Mathematics  
Mathematical Institute  
24 - 29 St Giles'  
Oxford  
OX1 3LB  
England



# Pebble bed: reflector treatment and pressure velocity coupling

Report prepared by J.P.F. Charpin, N. S. Kobo, K. Legodi, O.D. Makinde, J.-M. T. Ngnotchouye, H. Ockendon, A. Z. Owinoh, S. Peppin, J. Whiteley.

## Abstract

In this report, we describe some models and numerical methods used to simulate the flow and temperature in a pebble bed modular nuclear reactor. The reactor core is filled with around 450000 spheres containing low enriched uranium and helium is forced through these hot pebbles to cool the system down. The group first investigated the flow model in the pebbles. Numerical aspects were then considered to tackle difficulties encountered with the flow simulation and the temperature inside the pebbles. Numerical schemes are presented that can significantly improve the accuracy of the computed results.

## 1 Introduction and problem description

A pebble bed modular reactor (PBMR) is a gas cooled nuclear reactor of approximate cylindrical shape. The reactor core is filled with fuel pebbles containing low enriched uranium, located in an annular region close to the graphite centre of the reactor (figure 1). During the reaction, helium flows through the hot pebbles to cool down the system. The heat transferred to the gas is converted into electricity through a turbine. PBMR Ltd aims to perform real-time accurate simulations of the helium flow and temperature in the pebbles. This is currently achieved by calculating the values of the required parameters for a very limited number of points. They asked the group to investigate numerical difficulties they have encountered with the method they currently use. PBMR Ltd are looking for solutions that would allow them to keep their present finite volume numerical model on an unstructured grid.

Two types of numerical difficulties were encountered involving nonphysical variations in predicted velocities and temperatures at boundaries in the system. The first problem involves calculation of the flow of the hot gas. An abrupt change in the flow resistance is encountered when the gas enters the pebble bed. This causes unrealistic oscillations in the numerical solution around the gas-pebble interface. The second problem is related to simulations of heat flow between the pebble bed and reactor walls. Depending on the discretization used, large variations (up to 30 °C) in the temperature at the boundary are obtained. Refining the mesh removes the difference; however PBMR need to use a coarse mesh to enable real-time simulations. Both numerical difficulties have been resolved by a combination of related methods in the literature, and the development of new numerical methods based on integration and local analytical solutions. Details are given below, along with some thoughts on the appropriate physical modelling of the reactor core.

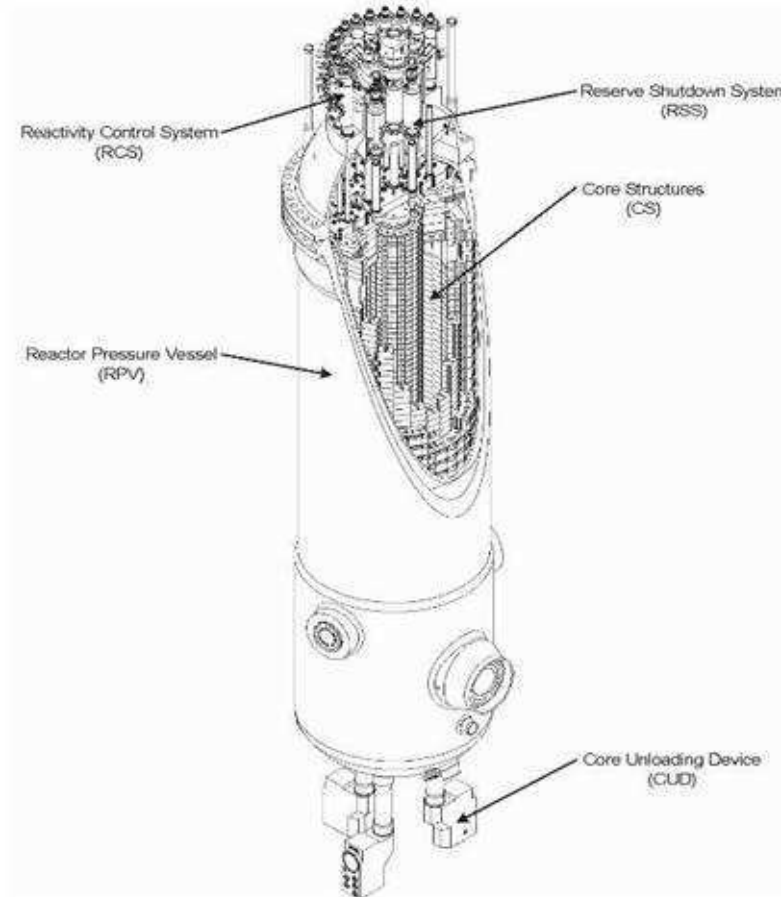


Figure 1: PBMR reactor.

## 2 Pressure velocity coupling

In this section we will investigate the numerical solution of the equations governing the transport of cooling gas through the nuclear reactor. We will first write down the equations (Section 2.1), before discussing issues with standard numerical schemes that have been used to solve these equations (Section 2.2). We will then discuss the application of a novel scheme to circumvent the difficulties encountered in Section 2.3. We will then conclude by briefly discussing other techniques that may be used to solve the governing equations.

### 2.1 The governing equations

The flow of gas through the nuclear reactor is modelled by the incompressible Navier–Stokes equations:

$$\rho \left( \frac{\partial \mathbf{u}}{\partial t} + (\mathbf{u} \cdot \nabla) \mathbf{u} \right) = -\nabla p + \mu \nabla^2 \mathbf{u} - \mathbf{S}, \quad \nabla \cdot \mathbf{u} = 0, \quad (1)$$

where  $\mathbf{S}$  is a momentum sink term and all other variables take their usual meanings. The main features that must be addressed may be illustrated using the one-dimensional, steady-state

form of equation (1):

$$\rho \frac{\partial}{\partial x} \left( \frac{1}{2} u^2 \right) = -\frac{\partial p}{\partial x} + \mu \frac{\partial^2 u}{\partial x^2} - S_x, \quad (2)$$

$$\frac{\partial u}{\partial x} = 0, \quad (3)$$

for  $-1 < x < 1$ , subject to boundary conditions

$$p(-1) = P_0, \quad p(1) = P_1, \quad (4)$$

where  $P_0 > P_1$ . The model system, equations. (2)–(4), is closed by specifying the momentum sink  $S_x$ . As suggested by Pebble Bed Modular Reactor (Pty) Limited (PBMR) we use

$$S_x = \begin{cases} k_0 u^2, & -1 < x < 0, \\ k_1 u^2, & 0 < x < 1. \end{cases} \quad (5)$$

The values of  $k_0$  and  $k_1$  are drastically different: this is a consequence of the gas flow meeting with a much higher resistance when flowing through regions of the reactor containing pebbles.

The system equations. (2)–(5) has exact solution

$$p = \begin{cases} P_0 - \rho k_0 u^2 (x + 1), & -1 < x < 0, \\ P_1 - \rho k_1 u^2 (x - 1), & 0 < x < 1, \end{cases}$$

$$u = \sqrt{\frac{P_0 - P_1}{\rho (k_0 + k_1)}}.$$

## 2.2 Standard numerical techniques

A common technique used for computing the numerical solution of the Navier–Stokes equations is the *finite volume technique*: see, for example, Tannehill *et al.* [1]. This method underpins the SIMPLE algorithm [2] which may be summarised as follows.

1. Guess the pressure field  $p_0$ .
2. Solve the momentum equation to calculate  $\mathbf{u}$ .
3. Use the continuity equation to update the pressure  $p$ .
4. Update the velocity field using  $\mathbf{u}_{new} = \mathbf{u}_{old} - A \nabla p$ .
5. Repeat steps 2–5 until the solution has converged.

PBMR have software that implements the SIMPLE algorithm. This software has much more functionality than fluid dynamics discussed here: as such PBMR are reluctant to implement significant changes to the fluid dynamics component of this software as it may impact elsewhere in the software. As a consequence, the SIMPLE algorithm must be implemented using a cell-centred finite volume method.

The drawback to implementing the SIMPLE algorithm using a cell-centred finite volume mesh is that the phenomenon known as *pressure–velocity uncoupling* occurs. This can sometimes be avoided by the use of Rhie–Chow interpolation [3]. However, this technique does not work well when there are rapid changes in body force, such as those appearing in our model problem in Section 2.1. When applied to the model problem, this technique induces “spikes” in the computed velocity rather than a constant velocity. This is demonstrated in Figure 2, where the computed velocity is shown by the solid line and the pressure shown by a broken line.

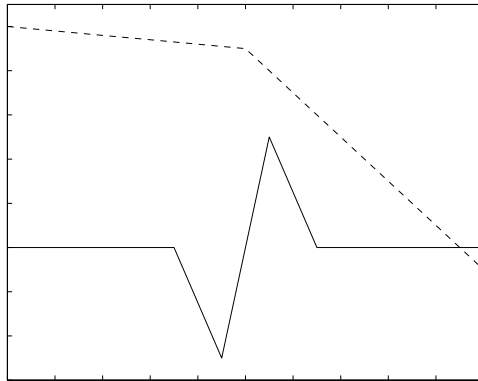


Figure 2: Velocity spikes: the solution of the model problem described in Section 2.1 using the SIMPLE algorithm with Rhie-Chow interpolation. The solid line represents the velocity, and the broken line represents the pressure.

### 2.3 A more appropriate numerical technique

The issue of velocity spikes was addressed by Mencinger and Žun [4] who modelled abrupt changes in the force field due to two mixed fluids, e.g. air bubbles in water. The key to this algorithm is the discretisation of the momentum sink: these terms should be discretised on the faces of the control volumes rather than at the cell centres. When this is done, the velocity spikes shown in Figure 2 are removed, and the velocity is given by a constant function as required.

This method appears to solve the problem encountered by PBMR, although there are some words of warning. As the momentum sink in equation (5) is dependent on  $\mathbf{u}$ , this quantity must first be calculated from the values at the cell-centres. Although this is not exactly what is desired by PBMR, it is likely to be a small modification to the code that is unlikely to cause any difficulties.

### 2.4 Discussion on pressure-velocity coupling

It should be noted that the SIMPLE algorithm was developed in 1980, and that the Rhie-Chow interpolation scheme was developed in 1983. The need to develop uncoupled algorithms such as these was largely dictated by computational resources—particularly memory—available at that time. However, the significant and steady increase in computer power that has been witnessed during the past 30 years has spawned the development of many more robust finite-volume and finite-element methods: although implementation of these methods would not have been possible on earlier machines, they are now the method of choice. Should PBMR ever decide to significantly overhaul their software they may wish to use these more robust algorithms.

## 3 Reflector treatment

The temperature in the pebble bed will now be studied. Two cases will be considered to solve the numerical difficulties encountered by PBMR Ltd:

- A simplified (non-physically realistic) solution where no heat may be transferred to the

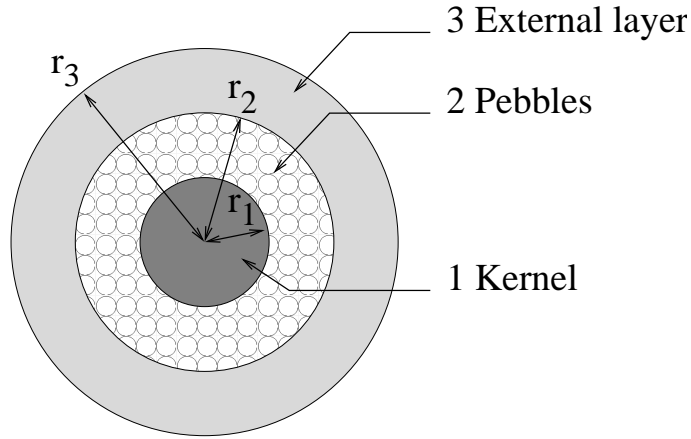


Figure 3: Simplified case configuration

gas. This case admits straightforward analytical solutions that considerably simplifies comparisons between analytical and numerical solutions.

- The complete system will then be considered. Analytical solutions involving Bessel functions are also available and the method developed for the simplified case will be extended.

### 3.1 Simplified case

The configuration studied in this section is presented in figure 3. Heat is only released in region 2 at the constant rate  $q$ . In this case, the governing equations may be written:

$$0 \leq r \leq r_1 \quad -\frac{1}{r} \frac{\partial}{\partial r} \left( \kappa_1 r \frac{\partial T}{\partial r} \right) = 0 \quad (6)$$

$$r_1 \leq r \leq r_2 \quad -\frac{1}{r} \frac{\partial}{\partial r} \left( \kappa_2 r \frac{\partial T}{\partial r} \right) = q \quad (7)$$

$$r_2 \leq r \leq r_3 \quad -\frac{1}{r} \frac{\partial}{\partial r} \left( \kappa_3 r \frac{\partial T}{\partial r} \right) = 0 \quad (8)$$

subject to the boundary conditions

$$T(r_3) = T_{ref}, \quad \left. \frac{\partial T}{\partial r} \right|_{r=0} = 0. \quad (9)$$

Using the continuity of temperatures and heat fluxes, the following analytical solution may be calculated:

$$\begin{aligned} 0 \leq r \leq r_1 \quad T &= T_0 - \frac{q}{2\kappa_3} (r_2^2 - r_1^2) \ln \left( \frac{r_2}{r_3} \right) - \frac{q}{4\kappa_2} (r_1^2 - r_2^2) \\ &\quad + \frac{qr_1^2}{2\kappa_2} \ln \left( \frac{r_1}{r_2} \right) \\ r_1 \leq r \leq r_2 \quad T &= T_0 - \frac{q}{2\kappa_3} (r_2^2 - r_1^2) \ln \left( \frac{r_2}{r_3} \right) - \frac{q}{4\kappa_2} (r^2 - r_2^2) \end{aligned} \quad (10)$$

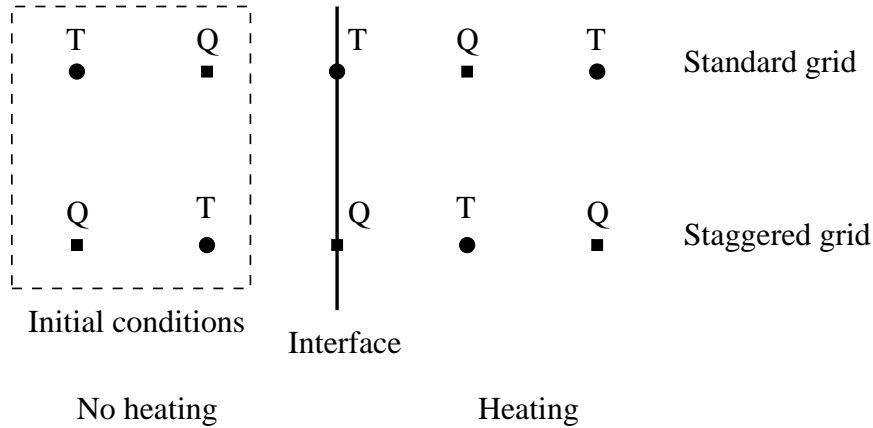


Figure 4: Typical grids

$$+ \frac{qr_1^2}{2\kappa_2} \ln\left(\frac{r}{r_2}\right) \quad (11)$$

$$r_2 \leq r \leq r_3 \quad T = T_0 - \frac{q}{2\kappa_3} (r_2^2 - r_1^2) \ln\left(\frac{r}{r_3}\right) \quad (12)$$

Numerical schemes are derived for the two types of grids described on figure 4. In each case, the space step is  $\Delta x$ . The position of the points will vary:

- Standard grids. The temperatures are calculated at positions  $x = i\Delta x$  and the fluxes are evaluated at  $x = (i + 1/2)\Delta x$ . The temperature  $T_i$  and the flux  $Q_{i+1/2}$  should be expressed as functions of  $T_{i-1}$  and  $Q_{i-1/2}$ .
- Staggered grids. The temperatures are calculated at positions  $x = (i + 1/2)\Delta x$  and the fluxes are evaluated at  $x = i\Delta x$ . The temperature  $T_{i+1/2}$  and the flux  $Q_i$  should be expressed as  $T_{i-1/2}$  and  $Q_{i-1}$ .

The objective here is to get the same quality of results on both grid types. The temperature will be calculated from the centre,  $r = 0$ ,  $i = 0$  towards the external boundary  $r_3$ ,  $n_3$ . Boundary conditions are at the two different extremities of the domain. In this simplified set-up, translating the temperature will not affect the result so the temperature  $T = 0$  may be imposed at the centre, and once the temperature profile has been determined, the results may be translated back so the boundary condition  $T(r_3) = T_{ref}$  is satisfied. The numerical scheme will be detailed for each of the three zones. Exact and approximated expressions are given for fluxes and temperatures in all possible cases.

### 3.1.1 Zone 1&3: Kernel and external layer

Integrating equation (6) or (8) between  $\alpha$  and  $r$  leads to:

$$\begin{aligned} \left[ \kappa r \frac{\partial T}{\partial r} \right] = 0 &\iff rQ = r_\alpha Q_\alpha \\ &\iff Q = \frac{r_\alpha}{r} Q_\alpha . \end{aligned}$$

Integrating the equation once more between  $a$  and  $b$  provides the relation:

$$T = T_a - \frac{r_\alpha Q_\alpha}{\kappa} \ln\left(\frac{r}{a}\right).$$

Using appropriate values of  $\alpha$ ,  $a$  and  $b$  leads to the following numerical schemes:

- Standard grid

$$\begin{aligned} Q_{i+1/2} &= \frac{r_{i-1/2}}{r_{i+1/2}} Q_{i-1/2} = Q_{i-1/2} \left(1 - \frac{\Delta r}{r_{i+1/2}}\right) + o(\Delta r^2) \\ T_{i+1} &= T_i - \frac{r_{i+1/2} Q_{i+1/2}}{\kappa} \ln\left(\frac{r_{i+1}}{r_i}\right) = T_i - \frac{Q_{i+1/2} \Delta r}{\kappa} + o(\Delta r^2) \end{aligned}$$

- Staggered grid

$$\begin{aligned} Q_i &= \frac{r_{i-1}}{r_i} Q_{i-1} = Q_{i-1} \left(1 - \frac{\Delta r}{r_i}\right) + o(\Delta r^2) \\ T_{i+1/2} &= T_{i-1/2} - \frac{r_i Q_i}{\kappa} \ln\left(\frac{r_{i+1/2}}{r_{i-1/2}}\right) = T_{i-1/2} - \frac{Q_i \Delta r}{\kappa} + o(\Delta r) \end{aligned}$$

### 3.1.2 Zone 2: Temperature in the pebbles

Similar integrations of equation (7) lead to the following equations

- Standard grid

$$\begin{aligned} Q_{i+1/2} &= \frac{r_{i-1/2}}{r_{i+1/2}} Q_{i-1/2} + q \frac{r_{i+1/2}^2 - r_{i-1/2}^2}{2r_{i+1/2}} \\ &= Q_{i-1/2} \left(1 - \frac{\Delta r}{r_{i+1/2}}\right) + q \Delta r - \frac{q \Delta r^2}{2r_{i+1/2}} + o(\Delta r^2) \\ T_{i+1} &= T_i + \left(\frac{q r_{i+1/2}^2}{2\kappa_2} - \frac{r_{i+1/2} Q_{i+1/2}}{\kappa_2}\right) \ln\left(\frac{r_{i+1}}{r_i}\right) - \frac{q}{4\kappa_2} (r_{i+1}^2 - r_i^2) \\ &= T_i - \frac{Q_{i+1/2} \Delta r}{\kappa_2} + o(\Delta r) \end{aligned}$$

- Staggered grid

$$\begin{aligned} Q_i &= \frac{r_{i-1}}{r_i} Q_{i-1} + q \frac{r_i^2 - r_{i-1}^2}{2r_i} = Q_{i-1} \left(1 - \frac{\Delta r}{r_i}\right) + q \Delta r - \frac{q \Delta r^2}{r_i} + o(\Delta r^2) \\ T_{i+1/2} &= T_{i-1/2} + \left(\frac{q r_i^2}{2\kappa_2} - \frac{r_i Q_i}{\kappa_2}\right) \ln\left(\frac{r_{i+1/2}}{r_{i-1/2}}\right) - \frac{q}{4\kappa_2} (r_{i+1/2}^2 - r_{i-1/2}^2) \\ &= T_{i-1/2} - \frac{Q_i \Delta r}{\kappa_2} + o(\Delta r) \end{aligned}$$

### 3.1.3 Interface zone 1-zone 2

The position of the interface is  $r_1 = i_1 \Delta r$ .

- Standard grid

$$\begin{aligned}
Q_{i_1+1/2} &= \frac{r_{i_1-1/2}}{r_{i_1+1/2}} Q_{i_1-1/2} + \frac{q}{2} \frac{r_{i_1+1/2}^2 - r_{i_1}^2}{r_{i_1+1/2}} \\
&= Q_{i_1-1/2} \left( 1 - \frac{\Delta r}{r_{i_1+1/2}} \right) + \frac{q}{2} \Delta r - \frac{q \Delta r^2}{8 r_{i_1+1/2}} + o(\Delta r^2) \\
T_{i_1+1} &= T_{i_1} + \frac{q r_{i_1+1/2}^2 / 2 - r_{i_1+1/2} Q_{i_1+1/2}}{\kappa_2} \ln \left( \frac{r_{i_1+1}}{r_{i_1}} \right) - \frac{q}{4 \kappa_2} (r_{i_1+1}^2 - r_{i_1}^2) \\
&= T_{i_1} - \frac{Q_{i_1+1/2} \Delta r}{\kappa_2} + o(\Delta r)
\end{aligned}$$

- Staggered grid

$$\begin{aligned}
Q_{i_1} &= \frac{r_{i_1-1}}{r_{i_1}} Q_{i_1-1} = Q_{i_1-1} \left( 1 - \frac{\Delta r}{r_{i_1}} \right) + o(\Delta r^2) \\
T_{i_1+1/2} &= T_{i_1-1/2} + \left( \frac{q r_{i_1}^2}{2 \kappa_2} - \frac{r_{i_1} Q_{i_1}}{\kappa_2} \right) \ln \left( \frac{r_{i_1+1/2}}{r_{i_1}} \right) - \frac{q}{4 \kappa_2} (r_{i_1+1/2}^2 - r_{i_1}^2) \\
&= T_{i_1-1/2} - \frac{Q_{i_1} \Delta r}{2 \kappa_2} + \left( \frac{Q_{i_1}}{8 r_{i_1} \kappa_2} - \frac{q}{8 \kappa_2} \right) \Delta r^2
\end{aligned}$$

### 3.1.4 Interface zone 2-zone 3

The position of the interface is  $r_2 = i_2 \Delta r$

- Standard grid

$$\begin{aligned}
Q_{i_2+1/2} &= \frac{r_{i_2-1/2}}{r_{i_2+1/2}} Q_{i_2-1/2} + \frac{q}{2} \frac{r_{i_2}^2 - r_{i_2-1/2}^2}{r_{i_2+1/2}} \\
&= Q_{i_2-1/2} \left( 1 - \frac{\Delta r}{r_{i_2+1/2}} \right) + \frac{q}{2} \Delta r - \frac{3q \Delta r^2}{8 r_{i_2+1/2}} + o(\Delta r^2) \\
T_{i_2+1} &= T_{i_2} - \frac{r_{i_2+1/2} Q_{i_2+1/2}}{\kappa_3} \ln \left( \frac{r_{i_2+1}}{r_{i_2}} \right) = T_{i_2} - \frac{Q_{i_2+1/2} \Delta r}{\kappa_3} + o(\Delta r)
\end{aligned}$$

- Staggered grid

$$\begin{aligned}
Q_{i_2} &= \frac{r_{i_2-1}}{r_{i_2}} Q_{i_2-1} + q \frac{r_{i_2}^2 - r_{i_2-1}^2}{2 r_{i_2}} = Q_{i_2-1} \left( 1 - \frac{\Delta r}{r_{i_2}} \right) + q \Delta r - \frac{q \Delta r^2}{2 r_{i_2}} + o(\Delta r^2) \\
T_{i_2+1/2} &= T_{i_2-1/2} - r_{i_2} Q_{i_2} \left[ \frac{1}{\kappa_2} \ln \left( \frac{r_{i_2}}{r_{i_2-1/2}} \right) + \frac{1}{\kappa_3} \ln \left( \frac{r_{i_2+1/2}}{r_{i_2}} \right) \right] + \frac{q r_{i_2}^2}{2 \kappa_2} \ln \left( \frac{r_{i_2}}{r_{i_2-1/2}} \right) \\
&\quad - \frac{q}{4 \kappa_2} (r_{i_2}^2 - r_{i_2-1/2}^2) \\
&= T_{i_2-1/2} - Q_{i_2} \Delta r \left( \frac{1}{2 \kappa_2} + \frac{1}{2 \kappa_3} \right) + \left( \frac{Q_{i_2}}{8 r_{i_2}} \left( \frac{1}{\kappa_3} - \frac{1}{\kappa_2} \right) + \frac{q}{8 \kappa_2} \right) \Delta r^2 + o(\Delta r^2)
\end{aligned}$$

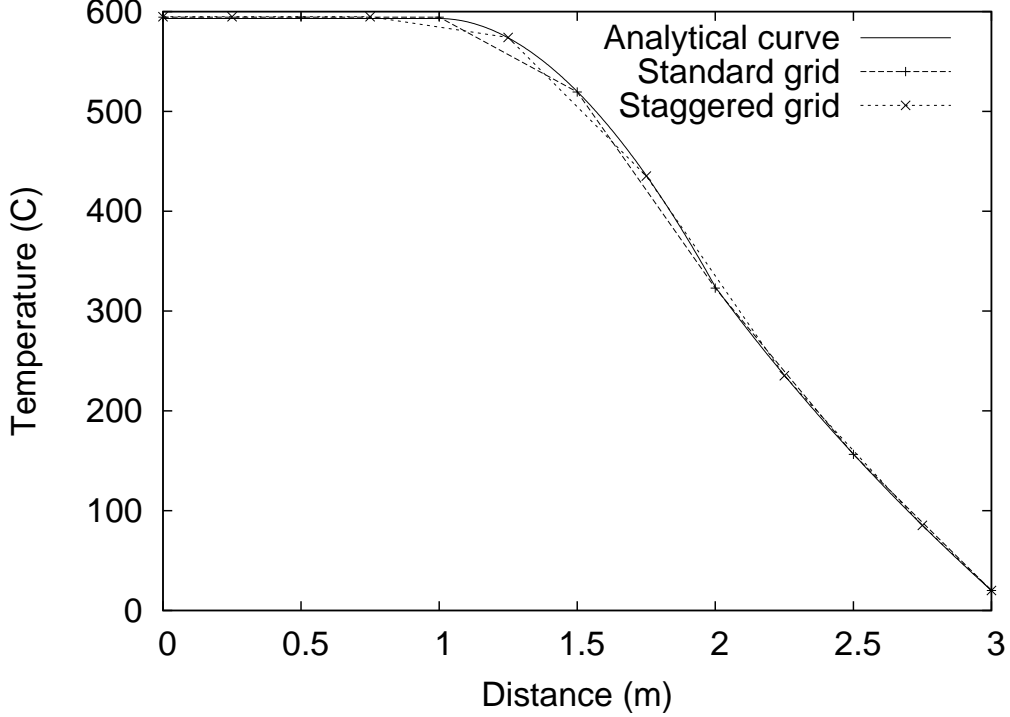


Figure 5: Comparison of the various schemes for the simplified model

### 3.1.5 Numerical results

Figure 5 compares the numerical results calculated with expansions and the analytical solution for the space step  $\Delta r = 0.5$ , which means 2 points per zone. The results are evaluated using first order approximations for the temperature and second order approximations for the fluxes. A second order approximation is also necessary at the interfaces for the staggered grid, otherwise, the heat produced in the pebbles would not influence the temperature on the cell. In this situation, the temperature calculated with either grid is very close to the analytical solution: the maximum difference observed occurs in the flat central region and is less than  $\Delta T \leq 2^\circ C$  for both curves. This difference is  $\Delta T \leq 0.5^\circ C$  if the number of points is doubled. Without second order expansions, for  $\Delta r = 0.5$  the difference between analytical and numerical results reaches  $\Delta T = 90^\circ C$  for the standard grid and  $\Delta T = 100^\circ C$  for the staggered grid. Using a second order approximation for the fluxes and the interfaces of the staggered grid is absolutely necessary to improve the accuracy of the numerical results.

## 3.2 Complete system

The complete configuration will now be studied. In this case, the governing equations may be written:

$$0 \leq r \leq r_1 \quad -\frac{1}{r} \frac{\partial}{\partial r} \left( \kappa_1 r \frac{\partial T}{\partial r} \right) = 0 \quad (13)$$

$$r_1 \leq r \leq r_2 \quad -\frac{1}{r} \frac{\partial}{\partial r} \left( \kappa_2 r \frac{\partial T}{\partial r} \right) = q + H (T_g - T) \quad (14)$$

$$r_2 \leq r \leq r_3 \quad -\frac{1}{r} \frac{\partial}{\partial r} \left( \kappa_3 r \frac{\partial T}{\partial r} \right) = 0 \quad (15)$$

subject to the boundary conditions

$$T(r_3) = T_{ref}, \quad \left. \frac{\partial T}{\partial r} \right|_{r=0} = 0. \quad (16)$$

Using the continuity of temperatures and heat fluxes, the following analytical solution may be calculated:

$$0 \leq r \leq r_1 \quad T = \alpha I_0 \left( r_1 \sqrt{\frac{H}{\kappa_2}} \right) + \beta K_0 \left( r_1 \sqrt{\frac{H}{\kappa_2}} \right) + \frac{q + HT_g}{H} \quad (17)$$

$$r_1 \leq r \leq r_2 \quad T = \alpha I_0 \left( r \sqrt{\frac{H}{\kappa_2}} \right) + \beta K_0 \left( r \sqrt{\frac{H}{\kappa_2}} \right) + \frac{q + HT_g}{H} \quad (18)$$

$$r_2 \leq r \leq r_3 \quad T = T_0 + \gamma \ln \left( \frac{r}{r_3} \right) \quad (19)$$

where  $I_0$  and  $K_0$  are the modified Bessel functions (see Appendix). The constants are defined by:

$$\begin{aligned} \alpha &= \frac{\kappa_3 \gamma}{r_2 \sqrt{H \kappa_2}} \frac{K_1 \left( r_1 \sqrt{(H/\kappa_2)} \right)}{I_1 \left( r_2 \sqrt{(H/\kappa_2)} \right) K_1 \left( r_1 \sqrt{(H/\kappa_2)} \right) - I_1 \left( r_1 \sqrt{(H/\kappa_2)} \right) K_1 \left( r_2 \sqrt{(H/\kappa_2)} \right)} \\ \beta &= \frac{\kappa_3 \gamma}{r_2 \sqrt{H \kappa_2}} \frac{I_1 \left( r_1 \sqrt{(H/\kappa_2)} \right)}{I_1 \left( r_2 \sqrt{(H/\kappa_2)} \right) K_1 \left( r_1 \sqrt{(H/\kappa_2)} \right) - I_1 \left( r_1 \sqrt{(H/\kappa_2)} \right) K_1 \left( r_2 \sqrt{(H/\kappa_2)} \right)} \\ \gamma &= \left( \frac{q + HT_g}{H} - T_0 \right) / \left( \ln \left( \frac{r_2}{r_3} \right) - \Delta \right) \\ \Delta &= \frac{\kappa_3}{r_2 \sqrt{H \kappa_2}} \frac{I_1 \left( r_1 \sqrt{(H/\kappa_2)} \right) K_0 \left( r_2 \sqrt{(H/\kappa_2)} \right) + I_0 \left( r_2 \sqrt{(H/\kappa_2)} \right) K_1 \left( r_1 \sqrt{(H/\kappa_2)} \right)}{I_1 \left( r_2 \sqrt{(H/\kappa_2)} \right) K_1 \left( r_1 \sqrt{(H/\kappa_2)} \right) - I_1 \left( r_1 \sqrt{(H/\kappa_2)} \right) K_1 \left( r_2 \sqrt{(H/\kappa_2)} \right)} \end{aligned}$$

and the functions  $I_1$  and  $K_1$  are modified Bessel functions defined in the Appendix. The numerical scheme will again be calculated for both standard and staggered grids. The schemes presented in the kernel and in the external layer remain unchanged. Inside the pebble zone, the flux and temperature may be expressed as

$$\begin{aligned} Q(r_d) &= Q_b \frac{I_1(r_d) K_0(r_a) + I_0(r_a) K_1(r_d)}{I_0(r_a) K_1(r_b) I_1(r_b) K_0(r_a)} \\ &\quad - \sqrt{H \kappa_2} \left( T_a - \frac{q + HT_g}{H} \right) \frac{I_1(r_d) K_1(r_b) - I_1(r_b) K_1(r_d)}{I_0(r_a) K_1(r_b) I_1(r_b) K_0(r_a)}, \\ T(r_c) &= \frac{q + HT_g}{H} + \left( T_a - \frac{q + HT_g}{H} \right) \frac{I_0(r_c) K_1(r_b) + I_0(r_b) K_1(r_c)}{I_0(r_a) K_1(r_b) I_1(r_b) K_0(r_a)} \\ &\quad + \frac{Q_b}{\sqrt{H \kappa_2}} \frac{I_0(r_a) K_0(r_c) - I_0(r_c) K_0(r_a)}{I_0(r_a) K_1(r_b) I_1(r_b) K_0(r_a)}, \end{aligned}$$

corresponding to the following boundary conditions:

$$T(r_a) = T_a, \quad Q(r_b) = Q_b.$$

These expressions are very long. The exact finite difference schemes will therefore not be written explicitly for each formula and the values of  $r_a$ ,  $r_b$ ,  $r_c$  and  $r_d$  will be given. Accuracy of the scheme may only be achieved when a third order approximation is used for the fluxes and temperatures at the boundaries. These expressions will be provided. A trial and error process is used to guarantee that the boundary conditions are satisfied.

### 3.2.1 Zone 2: temperature in the pebbles

- Standard grid

$r_a$	$r_b$	$r_d$
$r_i$	$r_i - \Delta r/2$	$r_i + \Delta r/2$

$$\begin{aligned}
Q_{i+1/2} &= -H \left( T_{i-1/2} - \frac{q - HT_g}{H} \right) \left( \Delta r - \frac{\Delta r^2}{2r_i} + \frac{\Delta r^3}{4r_i^2} + \frac{H\Delta r^3}{24\kappa_2} \right) \\
&\quad + Q_{i-1/2} \left( 1 - \frac{\Delta r}{r} + \frac{\Delta r^2}{2r_i^2} + \frac{H\Delta r^3}{24\kappa_2 r_i} - \frac{\Delta r^3}{4r_i^3} \right) + o(\Delta r^3) \\
T_{i+1} &= T_i - \frac{Q_{i+1/2}\Delta r}{\kappa_2} + o(\Delta r)
\end{aligned}$$

- Staggered grid

$r_a$	$r_b$	$r_d$
$r_i - \Delta r$	$r_i - 3\Delta r/2$	$r_i - \Delta r/2$

$$\begin{aligned}
Q_i &= Q_{i-1} \left( 1 - \frac{\Delta r}{r_i} + \frac{H\Delta r^3}{24\kappa_2 r_i} \right) \\
&\quad - H \left( T_{i-1/2} - \frac{q - HT_g}{H} \right) \left( \Delta r - \frac{\Delta r^2}{2r_i} - \frac{H\Delta r^3}{24\kappa_2} \right) + o(\Delta r^3) \\
T_{i+1/2} &= T_{i-1/2} - \frac{Q_i\Delta r}{\kappa_2} + o(\Delta r)
\end{aligned}$$

### 3.2.2 Interface zone 1-zone 2

- Standard grid

$r_a$	$r_b$	$r_d$
$r_{i_1}$	$r_{i_1}$	$r_{i_1} + \Delta r/2$

$$\begin{aligned}
Q_{i_1+1/2} &= -H \left( T_{i_1-1/2} - \frac{q - HT_g}{H} \right) \left( \frac{\Delta r}{2} - \frac{\Delta r^2}{8r_{i_1}} + \frac{H\Delta r^3}{48\kappa_2} + \frac{\Delta r^3}{16r_{i_1}^2} \right) \\
&\quad + Q_{i_1-1/2} \left( 1 - \frac{\Delta r}{2r_{i_1}} + \frac{H\Delta r^2}{8\kappa_2} + \frac{\Delta r^2}{4r_{i_1}^2} - \frac{H\Delta r^3}{24\kappa_2 r_{i_1}} - \frac{\Delta r^3}{24r_{i_1}^3} \right) + o(\Delta r^3) \\
T_{i_1+1} &= T_{i_1} - \frac{Q_{i_1+1/2}\Delta r}{\kappa_2} + o(\Delta r)
\end{aligned}$$

- Staggered grid

$r_a$	$r_b$	$r_c$	$r_d$
$r_{i_1}$	$r_{i_1}$	$r_{i_1} + \Delta r/2$	$r_{i_1} + \Delta r$

$$\begin{aligned}
Q_{i_1} &= \frac{r_{i_1-1}}{r_{i_1}} Q_{i_1-1} = Q_{i_1-1} \left( 1 - \frac{\Delta r}{r_{i_1}} \right) \\
T_{i_1+1/2} &= T_{i_1-1/2} + \left( \frac{HT_{i_1-1/2}}{\kappa_2} - \frac{q + HT_g}{\kappa_2} \right) \left( \frac{\Delta r^2}{8} - \frac{\Delta r^3}{48r_{i_1}} \right) \\
&\quad + \frac{Q_{i_1}}{\kappa_2} \left( \frac{\Delta r}{2} - \frac{3\Delta r^2}{8r_{i_1}} - \frac{H\Delta r^3}{24\kappa_2} + \frac{9\Delta r^3}{48r_{i_1}^2} \right) + o(\Delta r^3)
\end{aligned}$$

### 3.2.3 Interface zone 2-zone 3

- Standard grid

$r_a$	$r_b$	$r_d$
$r_{i_2}$	$r_{i_2} - \Delta r/2$	$r_{i_2}$

$$\begin{aligned}
Q_{i_2+1/2} &= -H \left( T_{i_2-1/2} - \frac{q - HT_g}{H} \right) \left( \frac{\Delta r}{2} - \frac{3\Delta r^2}{8r_{i_2}} - \frac{H\Delta r^3}{24\kappa_2} + \frac{3\Delta r^3}{16r_{i_2}^2} \right) \\
&\quad + Q_{i_2-1/2} \left( 1 - \frac{\Delta r}{r_{i_2}} + \frac{\Delta r^2}{r_{i_2}^2} - \frac{H\Delta r^2}{8\kappa_2} + \frac{7H\Delta r^3}{48\kappa_2 r_{i_2}} - \frac{\Delta r^3}{4r_{i_2}^3} \right) + o(\Delta r^3) \\
T_{i_2+1} &= T_{i_2} - \frac{Q_{i_2+1/2}\Delta r}{\kappa_3} + o(\Delta r)
\end{aligned}$$

- Staggered grid

$r_a$	$r_b$	$r_c$	$r_d$
$r_{i_2} - \Delta r/2$	$r_{i_2} - \Delta r$	$r_{i_2}$	$r_{i_2}$

$$\begin{aligned}
Q_{i_2} &= Q_{i_2-1} \left( 1 - \frac{\Delta r}{r_{i_2}} + \frac{H\Delta r^3}{24\kappa_2 r_{i_2}} \right) \\
&\quad - H \left( T_{i_2-1/2} - \frac{q - HT_g}{H} \right) \left( \Delta r - \frac{\Delta r^2}{2r_{i_2}} - \frac{H\Delta r^3}{24\kappa_2} \right) + o(\Delta r^3) \\
T_{i_2+1/2} &= T_{i_2-1/2} - \frac{H}{\kappa_2} \left( T_{i_2-1/2} - \frac{q - HT_g}{H} \right) \left( \frac{3\Delta r^2}{8} - \frac{7\Delta r^3}{48r_{i_2}} \right) \\
&\quad + \frac{Q_{i_2-1}}{\kappa_2} \left( -\frac{\Delta r}{2} + \frac{3\Delta r^2}{8r_{i_2}} + \frac{\Delta r^3}{12r_{i_2}^2} + \frac{H\Delta r^3}{24\kappa_2 r_{i_2}^2} \right) \\
&\quad + Q_{i_2} \left( \frac{\Delta r}{2\kappa_3} - \frac{\Delta r^2}{8\kappa_3 r_{i_2}} + \frac{\Delta r^3}{24\kappa_3 r_{i_2}^2} \right) + o(\Delta r^3)
\end{aligned}$$

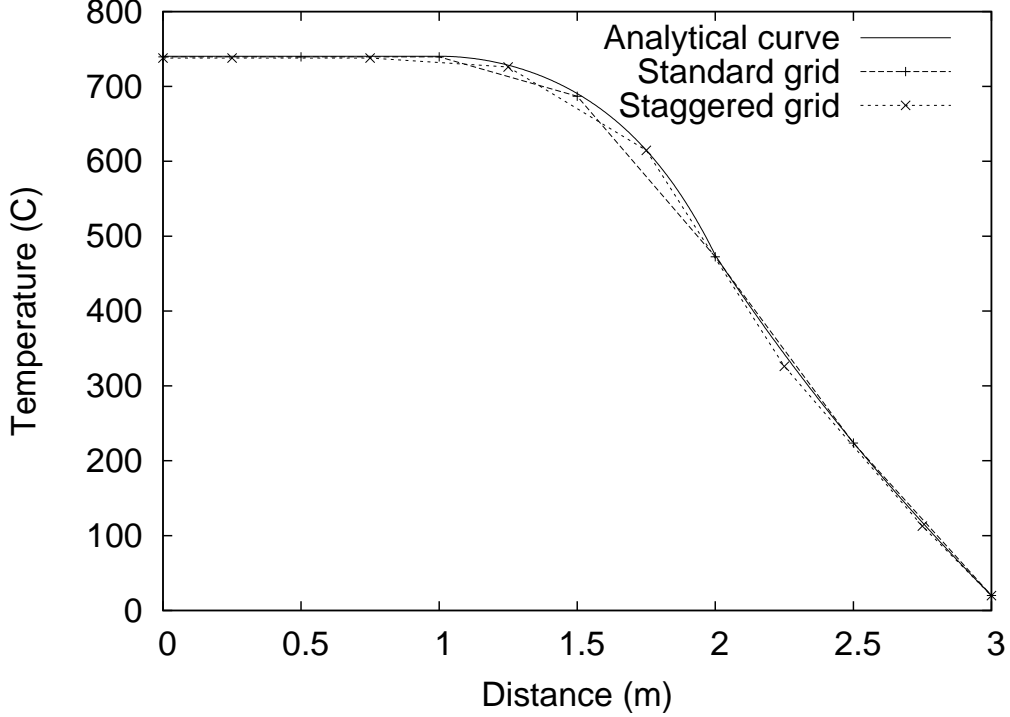


Figure 6: Comparison of the various schemes for the complete model

### 3.2.4 Numerical results

Figure 6 compares the numerical results calculated with expansions and the analytical solution for the space step  $\Delta r = 0.5$ , which again means two points per zone. The temperatures calculated with either grid are again really close to the analytical results. The differences is less than  $\Delta T = 4^\circ C$  for all points except for the staggered grid after the second interface, where the error is  $\Delta T = 16.5^\circ C$ . Here again, the error is reduced when the space step gets lower: the maximum error is  $\Delta T \leq 4.5^\circ C$  for  $\Delta r = 0.25$  with all other points except for one are calculated with an error less than  $\Delta T \leq 1.5^\circ C$ . The error is mainly due to the approximation of the flux. If accuracy may not be achieved with the third order accuracy for large values of the space step, using the exact solution of the flux could be a better option.

These results were calculated with gas temperature  $T_g = 700^\circ C$ . This temperature will vary significantly with the position in the vessel. This aspect will now be studied more carefully.

## 4 Temperature variation of gas in the pebbles

The temperature of the gas flow through the pebble bed will now be considered. We model the pebble bed reactor as a uniform channel with two distinct regions I & II, see figure 7. In region I, a cooling gas of temperature  $T_g$  flows with uniform velocity  $U$  towards region II which is occupied by pebbles. This region has a constant permeability,  $\epsilon$ , and heat source,  $q$ , and an adiabatic end. The temperature in region II is denoted  $T_p$ .

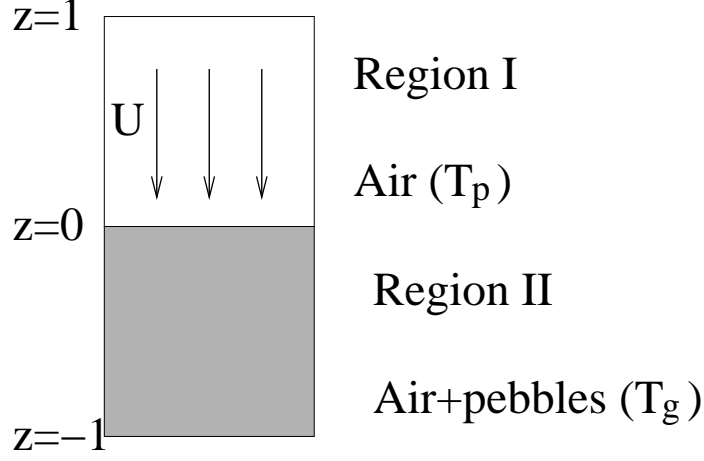


Figure 7: Simple geometry of the system

## 4.1 Model

For this one dimensional system, the steady state heat equations may be written:

$$\rho_g c_g U \frac{\partial T_g}{\partial z} = \kappa_g \frac{\partial^2 T_g}{\partial z^2} \quad \text{in Region I} \quad 0 \leq z \leq 1, \quad (20)$$

$$\rho_g c_g \frac{U}{\epsilon} \frac{\partial T_p}{\partial z} = \kappa_g \frac{\partial^2 T_p}{\partial z^2} + q \quad \text{in Region II} \quad -1 \leq z \leq 0, \quad (21)$$

and all the quantities are defined in the Nomenclature section. To simplify the problem, all quantities are assumed constant. Equations (20–21) are solved subject to the following boundary conditions:

- Imposed temperature at the top:

$$T_g(L) = T_0 ,$$

- Adiabatic condition at the bottom:

$$\left. \frac{\partial T_p}{\partial z} \right|_{z=-L} = 0 ,$$

- Continuity of temperature and fluxes at the interface

$$\begin{aligned} T_g(0) &= T_p(0) \\ \left. \frac{\partial T_g}{\partial z} \right|_{z=0} &= \left. \frac{\partial T_p}{\partial z} \right|_{z=0} . \end{aligned}$$

The flux condition may be simplified since the conduction is the same on either side of the interface.

The length and temperature are non dimensionalised as follows:

$$z = Lz' , \quad T = T_0 + \Delta T T' ,$$

where  $L$  is the typical height,  $T_0$  is the initial temperature of the gas and  $\Delta T$  a typical temperature gap. The governing equations become

$$\begin{aligned}\frac{\partial T_g}{\partial z} &= \frac{\kappa_g}{\rho_g c_g L U} \frac{\partial^2 T_g}{\partial z^2}, \\ \frac{\partial T_p}{\partial z} &= \frac{\epsilon \kappa_g}{\rho_g c_g L U} \frac{\partial^2 T_p}{\partial z^2} + \frac{\epsilon L q}{\rho_g c_g \Delta T U}.\end{aligned}$$

Clearly, the temperature is governed by convection and the heat source, so the typical temperature gap is

$$\Delta T = \frac{\epsilon L q}{\rho_g c_g U}.$$

The governing equations are then

$$\frac{\partial T_g}{\partial z} = \kappa_1 \frac{\partial^2 T_g}{\partial z^2}, \quad (22)$$

$$\frac{\partial T_p}{\partial z} = \epsilon \kappa_1 \frac{\partial^2 T_p}{\partial z^2} + 1, \quad (23)$$

subject to the boundary condition

$$T_g(1) = 0, \quad (24)$$

$$\left. \frac{\partial T_p}{\partial z} \right|_{z=-1} = 0, \quad (25)$$

$$T_g(0) = T_p(0) \quad (26)$$

$$\left. \frac{\partial T_g}{\partial z} \right|_{z=0} = \left. \frac{\partial T_p}{\partial z} \right|_{z=0}, \quad (27)$$

where

$$\kappa_1 = \frac{\kappa_g}{\rho_g c_g L U}.$$

Equations (22–27) may be solved easily:

$$T_g = A + B e^{z/\kappa_1}, \quad (28)$$

$$T_p = C + D e^{z/(\epsilon \kappa_1)} + z, \quad (29)$$

where

$$A = \kappa_1 e^{1/\kappa_1} (e^{1/(\epsilon \kappa_1)} - 1)$$

$$B = \kappa_1 (1 - e^{1/(\epsilon \kappa_1)})$$

$$C = \epsilon \kappa_1 e^{1/(\epsilon \kappa_1)} + \kappa_1 (1 - e^{1/(\epsilon \kappa_1)}) (1 - e^{1/\kappa_1})$$

$$D = -\epsilon \kappa_1 e^{1/(\epsilon \kappa_1)}.$$

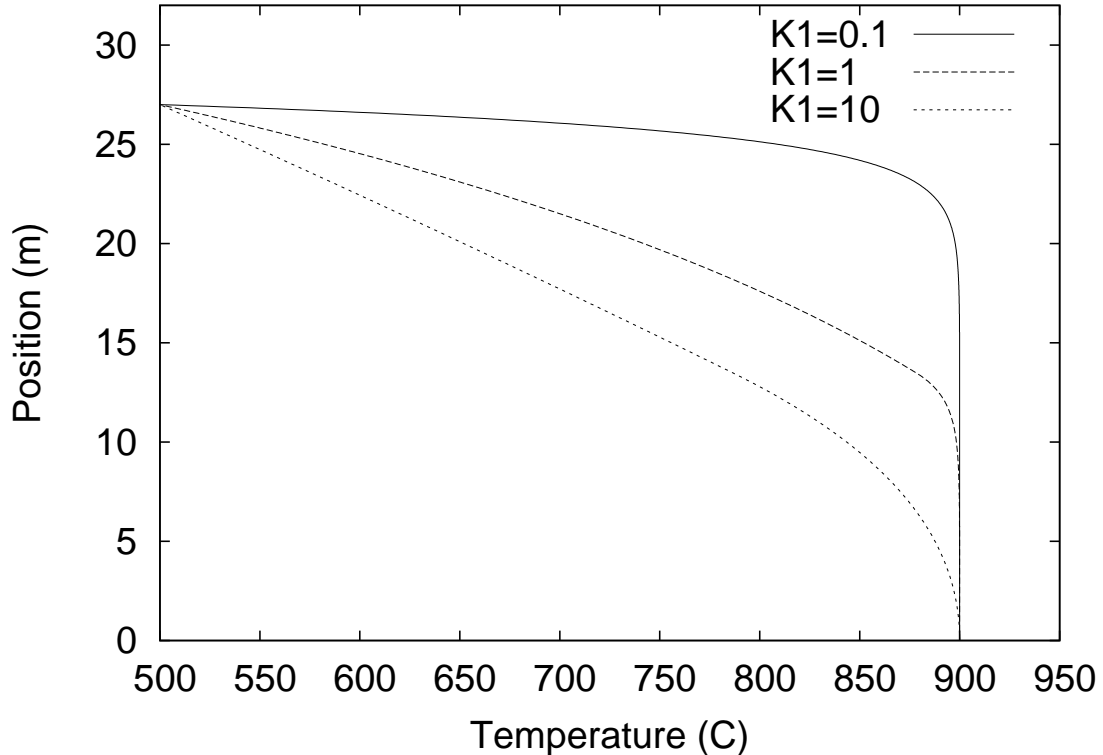


Figure 8: Gas temperature profiles for various values of  $\kappa_1$

## 4.2 Numerical results

The temperature of the air is plotted in figure 8 for  $\kappa_1 = 0.1, 1, 10$ . The results are dimensionalised to fit with experimental results: at the top of the pressure vessel, the temperature is  $T = 500^\circ\text{C}$  and at the bottom  $T = 900^\circ\text{C}$ . These curves correspond to  $\epsilon = 0.1$ . The curves calculated with  $\epsilon = 0.3$  are very close to the curves obtained in figure 8. The parameter  $\kappa_1$  seems to have more influence. The value of this parameter depends on the thermal properties of the gas and the velocity of the gas. These values were taken constant but should vary with the gas temperature and pressure. The results are therefore only a first approximation.

## 5 Conclusion and future work

The study group provided insights on the gas flow model inside the pebbles and suggested solutions for the numerical problems encountered by PBMT Ltd.

- The velocity spikes observed numerically at the surface of the pebbles may be removed by employing an adequate numerical method. The crux of the problem is the discretisation of the sink terms: they should be evaluated at the boundaries of the grid cells and not at the centre.
- The numerical problems due to the two different types of grids may be solved by using specially designed numerical schemes. To achieve maximum accuracy, the formulae should be based on local analytical solutions of the governing equations. They can be approximated using Taylor series expansions. Depending on the position and parameter,

first second or third order Taylor expansions are required to guarantee that the numerical solutions are close enough to the analytical solution.

Temperature in the pebbles was calculated in each cross section of the pressure vessel. The evolution of the temperature in the axis direction was neglected, although this was shown to vary significantly. Vertical heat conduction should be investigated to further increase the accuracy of the numerical simulations

## Acknowledgements

J.P.F. Charpin acknowledges the support of the Mathematics Application Consortium for Science and Industry ([www.macsi.ul.ie](http://www.macsi.ul.ie)) funded by the Science Foundation Ireland mathematics initiative Grant No 06/MI/005.

## References

- [1] J.C. Tannehill, D.A. Anderson, and R.H. Pletcher. *Computational Fluid Mechanics and Heat Transfer*. Taylor & Francis, Philadelphia, PA, USA, 1997.
- [2] S.V. Patankar. *Numerical Heat Transfer and Fluid Flow*. Hemisphere Publishing Corporation, 1980.
- [3] C.M. Rhie and W.L. Chow. Numerical study of the turbulent flow past an airfoil with trailing edge separation. *AIAA Journal*, 21:1525–1532, 1983.
- [4] J. Mencinger and I. Žun. On the finite volume discretization of discontinuous body force field on collocated grid: Application to VOF method. *Journal of Computational Physics*, 221:524–538, 2007.

# Nomenclature

$\alpha$	heat transfer coefficient		$\text{W}\cdot\text{m}^{-2}\cdot\text{K}^{-1}$
$\epsilon$	Porosity coefficient	0 – 1	ND
$\kappa$	Thermal conductivity	$\kappa_1 = 10, \kappa_2 = 15,$ $\kappa_3 = 20$	$\text{W}\cdot\text{m}^{-1}\cdot\text{K}^{-1}$
$\mu$	Dynamic viscosity		$\text{kg}\cdot\text{m}^{-1}\cdot\text{s}^{-1}$
$\rho$	Density		$\text{kg}\cdot\text{m}^{-3}$
$\Delta r, \Delta x, \Delta y$	Space steps in the r, x and y directions		m
$c$	Heat capacity		$\text{J}\cdot\text{kg}^{-1}\cdot\text{K}^{-1}$
$p$	Pressure		Pa
$q$	Heat source	10000	$\text{W}\cdot\text{m}^{-3}$
$r, x, y$	Radial and Cartesian coordinates		m
$t$	Time		s
$\vec{v} = (u, v)$	Velocity in x and y directions		$\text{m}\cdot\text{s}^{-1}$
$H$	Non standard heat transfer coefficient		$\text{W}\cdot\text{m}^{-3}\cdot\text{K}^{-1}$
$Q$	Heat flux		$\text{W}\cdot\text{m}^{-2}$
$Re$	Reynolds number		
$S = (S_x, S_y)$	Momentum sink term		$\text{m}\cdot\text{s}^{-2}$
$T$	Temperature		K
$U$	Gas velocity		$\text{m}\cdot\text{s}^{-1}$

Under scripts

$p$ , Pebbles,  
 $g$ , Gas.

## A Bessel functions

Bessel functions were used in section 3. These function are defined as follows:

$$\begin{aligned}
 I_0(x) &= \sum_{k=0}^{\infty} \frac{z^{2k}}{4^k (k!)^2}, \\
 I_1(x) &= I_0'(x) = \sum_{k=1}^{\infty} \frac{(2k)z^{2k-1}}{4^k (k!)^2}, \\
 K_0(x) &= -I_0(x) \left[ \ln\left(\frac{x}{2}\right) + \gamma \right] + \sum_{k=1}^{\infty} \frac{z^{2k} \psi(k)}{4^k (k!)^2}, \\
 K_1(x) &= -K_0'(x) = I_1(x) \left[ \ln\left(\frac{x}{2}\right) + \gamma \right] + \frac{I_0(x)}{x} - \sum_{k=1}^{\infty} \frac{(2k)z^{2k-1} \psi(k)}{4^k (k!)^2},
 \end{aligned}$$

where  $\gamma = 0.57721566$  is the Euler constant and

$$\psi(k) = \sum_{i=1}^k \frac{1}{i}.$$

In the present code, the functions were approximated using sums up to  $k_{max} = 30$ .



## RECENT REPORTS

### 2009

01/09	A Mass and Solute Balance Model for Tear Volume and Osmolarity in The Normal And The Dry Eye	Gaffney Tiffany Yokoi Bron
02/09	Diffusion and permeation in binary solutions	Peppin
03/09	On the modelling of biological patterns with mechanochemical models: insights from analysis and computation	Moreo Gaffney Garcia-Aznar Doblare
04/09	Stability analysis of reaction-diffusion systems with time-dependent coefficients on growing domains	Madzvamuse Gaffney Maini
05/09	Onsager reciprocity in premelting solids	Peppin Spannuth Wettlaufer
06/09	Inherent noise can facilitate coherence in collective swarm motion	Yates <i>et al.</i>
07/09	Solving the Coupled System Improves Computational Efficiency of the Bidomain Equations	Southern Plank Vigmond Whiteley
08/09	Model reduction using a posteriori analysis	Whiteley
09/09	Equilibrium Order Parameters of Liquid Crystals in the Landau-De Gennes Theory	Majumdar
10/09	Landau-De Gennes theory of nematic liquid crystals: the Oseen-Frank limit and beyond	Majumdar Zarnescu
11/09	A Comparison of Numerical Methods used for Finite Element Modelling of Soft Tissue Deformation	Pathmanathan Gavaghan Whiteley
12/09	From Individual to Collective Behaviour of Unicellular Organisms: Recent Results and Open Problems	Xue Othmer Erban
13/09	Stochastic modelling of reaction-diffusion processes: algorithms for bimolecular reactions	Erban Chapman
14/09	Chaste: a test-driven approach to software development for physiological modelling	Pitt-Francis <i>et al.</i>

15/09	Block triangular preconditioners for PDE constrained optimization	Rees Stoll
16/09	From microscopic to macroscopic descriptions of cell migration on growing domains	Baker Yates Erban
17/09	The Influence of Gene Expression Time Delays on Gierer-Meinhardt Pattern Formation Systems	Seirin Lee Gaffney Monk
18/09	Analysis of a stochastic chemical system close to a sniper bifurcation of its mean field model	Erban <i>et al.</i>
19/09	On the existence and the applications of modified equations for stochastic differential equations	Zygalakis

**Copies of these, and any other OCCAM reports can be obtained from:**

**Oxford Centre for Collaborative Applied Mathematics  
Mathematical Institute  
24 - 29 St Giles'  
Oxford  
OX1 3LB  
England**

**[www.maths.ox.ac.uk/occam](http://www.maths.ox.ac.uk/occam)**